

UC Berkeley

UC Berkeley Previously Published Works

Title

Van Krevelen diagrams based on machine learning visualize feedstock-product relationships in thermal conversion processes.

Permalink

<https://escholarship.org/uc/item/3qx99782>

Journal

Communications Chemistry, 6(1)

Authors

Wang, Shule

Wang, Yiyi

Shi, Ziyi

et al.

Publication Date

2023-12-13

DOI







10.1038/s42004-023-01077-z

Copyright Information

This work is made available under the terms of a Creative Commons Attribution License, available at <https://creativecommons.org/licenses/by/4.0/>

Peer reviewed

Van Krevelen diagrams based on machine learning visualize feedstock-product relationships in thermal conversion processes

Shule Wang ^{1,2,14}, Yiyang Wang^{3,14}, Ziyi Shi^{4,14}, Kang Sun^{1,2,14}, Yuming Wen ^{3✉}, Lukasz Niedzwiecki ^{5,6}, Ruming Pan ^{7,8}, Yongdong Xu⁹, Ilman Nuran Zaini⁴, Katarzyna Jagodzińska⁴, Christian Aragon-Briceno¹⁰, Chuchu Tang¹¹, Thossaporn Onsree¹², Nakorn Tippayawong¹³, Halina Pawlak-Kruczek⁵, Pär Göran Jönsson⁴, Weihong Yang⁴, Jianchun Jiang ^{1,2✉}, Sibudjing Kawi ^{3✉} & Chi-Hwa Wang^{3✉}

Feedstock properties play a crucial role in thermal conversion processes, where understanding the influence of these properties on treatment performance is essential for optimizing both feedstock selection and the overall process. In this study, a series of van Krevelen diagrams were generated to illustrate the impact of H/C and O/C ratios of feedstock on the products obtained from six commonly used thermal conversion techniques: torrefaction, hydrothermal carbonization, hydrothermal liquefaction, hydrothermal gasification, pyrolysis, and gasification. Machine learning methods were employed, utilizing data, methods, and results from corresponding studies in this field. Furthermore, the reliability of the constructed van Krevelen diagrams was analyzed to assess their dependability. The van Krevelen diagrams developed in this work systematically provide visual representations of the relationships between feedstock and products in thermal conversion processes, thereby aiding in optimizing the selection of feedstock and the choice of thermal conversion technique.

¹Jiangsu Province Key Laboratory of Biomass Energy and Materials, National Engineering Laboratory for Biomass Chemical Utilization, Institute of Chemical Industry of Forest Products, Chinese Academy of Forestry (CAF), 210042 Nanjing, China. ²Jiangsu Co-Innovation Center for Efficient Processing and Utilization of Forest Resources, College of Chemical Engineering, Nanjing Forestry University, Longpan Road 159, 210037 Nanjing, China. ³Department of Chemical and Biomolecular Engineering, National University of Singapore, 4 Engineering Drive 4, Singapore 117585, Singapore. ⁴Department of Materials Science and Engineering, KTH Royal Institute of Technology, SE-100 44 Stockholm, Sweden. ⁵Department of Energy Conversion Engineering, Wrocław University of Science and Technology, 27 wybrzeże Stanisława Wyspiańskiego st. 50-370, Wrocław, Poland. ⁶Energy Research Centre, Centre for Energy and Environmental Technologies, VŠB-Technical University of Ostrava, 708 00 Ostrava, Poruba, Czech Republic. ⁷School of Energy Science and Engineering, Harbin Institute of Technology, 150001 Harbin, China. ⁸Institut de Mécanique des Fluides de Toulouse (IMFT) - Université de Toulouse, CNRS-INPT-UPS, 31400 Toulouse, France. ⁹Laboratory of Environment-Enhancing Energy (E2E), Key Laboratory of Agricultural Engineering in Structure and Environment of Ministry of Agriculture and Rural Affairs, China Agricultural University, 100083 Beijing, China. ¹⁰Department of Industry and Energy, CIRCE-Research Centre for Energy Resources and Consumption, 50018 Zaragoza, Spain. ¹¹Faculty of Creative Arts, University of Malaya, 50603 Kuala Lumpur, Malaysia. ¹²Department of Chemical Engineering, University of South Carolina, 301 Main St, Columbia, SC 29208, USA. ¹³Department of Mechanical Engineering, Chiang Mai University, 239 Huay Kaew Rd., Muang District, Chiang Mai 50200, Thailand. ¹⁴These authors contributed equally: Shule Wang, Yiyang Wang, Ziyi Shi, Kang Sun. ✉email: yuming@nus.edu.sg; jiangjc@caf.ac.cn; chekawis@nus.edu.sg; chewch@nus.edu.sg

The thermal conversion process, also known as the thermochemical process, has been widely developed and utilized for treating waste/biomass during recent decades^{1,2}. These thermal conversion techniques offer options for power generation, fuel production, and chemical synthesis from different feedstocks³. Combustion, as a prevalent thermal conversion process, has been extensively studied and well-understood in terms of energy production and resulting by-products⁴. Emerging techniques such as torrefaction, pyrolysis, gasification, and hydrothermal liquefaction (HTL) have received more attention and present more complex performance dynamics^{5,6}.

The feedstock properties used in thermal conversion processes play a critical role in their performance. As a result, numerous studies have been conducted to investigate the performance of different thermal conversion processes using various raw materials⁷, requiring significant research resources. The complexity of feedstock composition hinders researchers from identifying general principles through experimental studies. Having a simple model or guidance tool that can provide a preliminary estimation of thermal conversion process behavior based on feedstock properties would facilitate and accelerate the research and decision-making processes. Such a tool could indicate the relationship between the feedstock properties and the quantity and quality of products obtained from thermal conversion processes. Additionally, it could serve two practical objectives: guiding the selection of a suitable thermal conversion technique for a specific feedstock and assisting in determining the optimal feedstock or blend for a particular thermal conversion technique.

The van Krevelen diagram, introduced by Dirk Willem van Krevelen in 1950⁸, displays the atomic ratios of H/C and O/C and was originally used to illustrate humification and coal formation processes visually⁹. Over time, it has been recognized as a useful tool for estimating main compound categories and reflecting their calorific values¹⁰. Consequently, its application has expanded beyond coal, denoting relevant properties of diverse materials, including biomass, biodegradable waste, and various chemicals, both pre- and post-reactions^{11–19}.

In the field of thermal conversion, the van Krevelen diagram has been widely used to intuitively indicate differences in H/C and O/C ratios among feedstocks and products in processes such as torrefaction²⁰, hydrothermal carbonization²¹, pyrolysis²², and gasification²³. This application provides a unique way to visually illustrate the directions of not only thermal conversions but also other chemical reactions^{24–28}. However, real feedstocks, such as biomass and biodegradable waste, are typically mixtures, implying that numerous reactions can occur during the thermal conversion process. Consequently, previous investigations using the van Krevelen diagram to understand the directions of several specific reactions can be challenging to apply to the analysis of mixtures. On the other hand, although there have been studies using the van Krevelen diagram to illustrate the thermal conversion reactions of real biomass and biodegradable wastes such as algae²⁹, lignocellulosic biomass³⁰, and digestate³¹, typically only single or a few cases are reported in each study. Therefore, there is interest in addressing these gaps and creating van Krevelen diagrams that better reflect the real-world applications of different thermal conversion techniques.

Machine learning (ML) has become widely used in various fields³², including constructing models for thermal conversion processes^{33,34}. In most of the reported ML studies of thermal processes, the constructed ML model can predict the output from given input parameters with a coefficient of determination (R^2) higher than 0.8³³. One ML interpretation method, the partial dependence plot, can be used to evaluate the marginal effects of selected input variables on the output value³⁵. By using the H/C and O/C ratios of feedstocks as input parameters for an ML

model and plotting the two-way partial dependence of these input variables on the output value, a three-dimensional van Krevelen diagram can be created. It will be promising to use the ML method to construct the van Krevelen diagram: using the database yielded from experiments with mixture feedstock will give insight into the corresponding thermal process to treat real feedstock.

In this analysis, we create a series of van Krevelen diagrams to illustrate the relationship between the feedstock and its thermal conversion products through ML analysis of eight corresponding ML studies (Fig. 1). We analyze the constructed van Krevelen diagrams theoretically and propose suggestions for applying different thermal conversion processes to treat waste/biomass based on the diagrams generated. The reliabilities of the constructed diagrams are discussed. The study demonstrates that the constructed van Krevelen diagrams can effectively represent the feedstock-product relationship of part of the thermal conversion processes and can serve as an important reference for decision-making in different applications.

Results and discussion

Construction of van Krevelen diagram. Figure 1 depicts the process of constructing and analyzing a van Krevelen diagram, using the yield of pyrolysis oil as an example. The database used for constructing the diagram is sourced from a precious study³⁶ and revised accordingly. Among the eight referenced studies, the random forest method has been implemented most frequently, with a testing R^2 value greater than 0.75 (as shown in Fig. 1). To establish a set of general diagrams for different thermal conversion processes, we consistently employ the random forest method verified its performance using the Leave One Out method (90% train data and 10% test data). The model is constructed using the scikit-learn 0.23.1 library in a Python 3 environment and details are given in Supplementary Note 4.

To generate the van Krevelen diagram, a two-way partial dependence analysis is performed based on the constructed model, focusing on the H/C and O/C ratios. The reliability of the produced diagram is highest within the ranges where the training data is most abundant. The dataset was initially collected from reported experimental works. In these experiments, researchers often explored various thermal conversion process parameters for a single feedstock. Therefore, plotting the H/C and O/C ranges for the collected data cannot accurately represent the true density of the dataset. To address this, we apply the kernel density of the training data to determine the appropriate ranges for the van Krevelen diagrams. The kernel density plots created for all datasets are given in Supplementary Figs. 7–10.

During the analysis, all other input parameters are set to their mean values from the training dataset. The resulting two-way partial dependence plots represent the predicted outcomes under specific input conditions. To obtain a van Krevelen diagram that can represent the relationship between feedstock and product more generally, smoothing is applied to the original two-way partial dependence plots. The detailed setting of smoothing is given in Supplementary Fig. 5.

The thermal conversion reaction models for individual feedstocks, such as cellulose, have been well developed. However, in real-world scenarios, raw materials are typically mixtures. This study demonstrates that machine learning methods can be utilized to capture the complexities of reactions involving mixed feedstocks (Supplementary Note 1). It's important to note that elements in the feedstock other than C, H, and O can significantly influence the properties of the final product, such as its ash content (Supplementary Note 2). However, this study focuses solely on the C, H, and O contents, as they are the most abundant

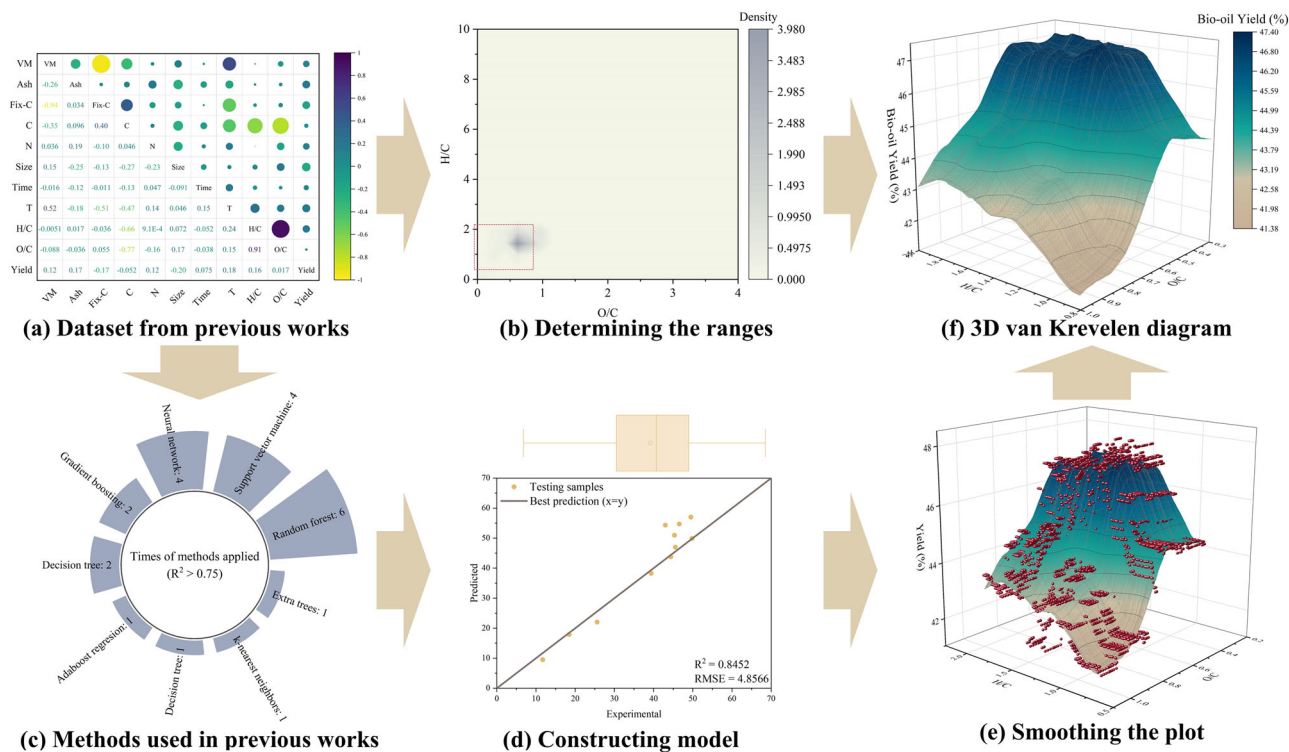


Fig. 1 Schematic of the construction and analysis of van Krevelen diagrams. Using the yield of pyrolysis oil as an example. a Pearson correlation of the raw dataset³⁶. **b** Kernel density diagram for determination of the range of the predicting area. **c** The ML methods used in collected literature. **d** The fitting diagram of trained model. **e** Plot smoothing of the 2D-partial dependence plot which used H/C and O/C as axis. **f** The ascended 3D van Krevelen diagram.

elements in organic feedstocks. Considering the intricate nature of feedstocks, the complexity further intensifies when aiming to produce chemical products (Supplementary Note 3). Therefore, this study focuses on analyzing the fuel properties of thermal conversion products.

Torrefaction. During torrefaction, partial devolatilization occurs, leading to a decrease in volatile matter content^{20,37}. This process makes the torrefied material more similar to coal compared to unprocessed biomass. Figure 2 demonstrates a generally negative correlation between the H/C and O/C ratios of the feedstock and the solid yield from biomass torrefaction, with a stronger correlation observed for the H/C ratio. The trend aligns with findings in the literature^{37,38} and can be attributed to the composition of lignocellulosic biomass, particularly the hemicellulose content. Hemicellulose and cellulose have higher H/C and O/C ratios compared to lignin³⁷. Thus, as the hemicellulose content increases in the raw biomass, the H/C and O/C ratios of the biomass also increase. The main mechanisms involved in biomass torrefaction are dehydration and decarboxylation³⁹. Hemicellulose, which contains abundant hydroxyl groups, undergoes degradation during torrefaction through dehydration and the breaking of weak linkages between small substituents and the main polymer chains⁴⁰. Generally, due to its lower thermal stability compared to cellulose and lignin⁴¹, hemicellulose decomposition prevails at lower temperatures, such as in torrefaction. Therefore, a higher hemicellulose content results in more intense devolatilization and, ultimately, a lower solid yield from the process for the same severity of the torrefaction process⁴².

Hydrothermal processes

Hydrothermal carbonization (HTC). The reactions during HTC involve hydrolysis, dehydration, decarboxylation, condensation,

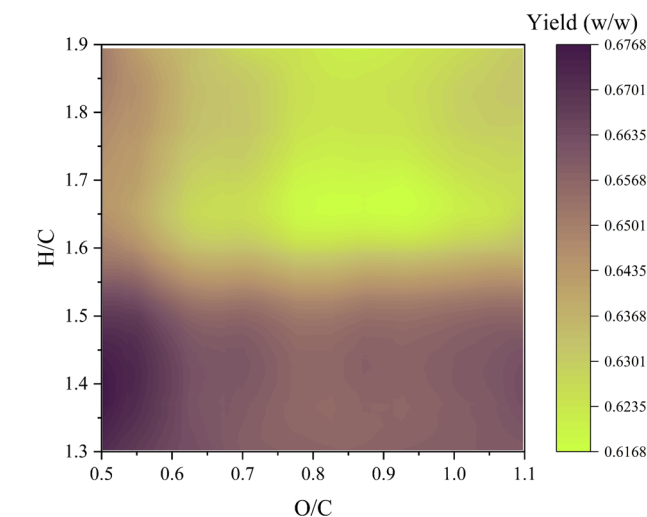


Fig. 2 Van Krevelen diagram for torrefaction product. The diagram is constructed based on previous work by Onsee et al.⁷⁰ The feedstock investigated is lignocellulosic biomass, including agricultural and forestry residues, as well as energy crops. The x-axis and y-axis represent the O/C and H/C of feedstock, respectively, while the z-axis indicates the yield of the product.

polymerization, aromatization, and condensation, among others⁴³. Dehydration and decarboxylation are the primary mechanisms in HTC⁴⁴. Consequently, higher H/C and O/C ratios in the feedstock result in higher H/C and O/C ratios in the produced hydrochar, as shown in the HTC H/C and H/O diagrams (Fig. 3).

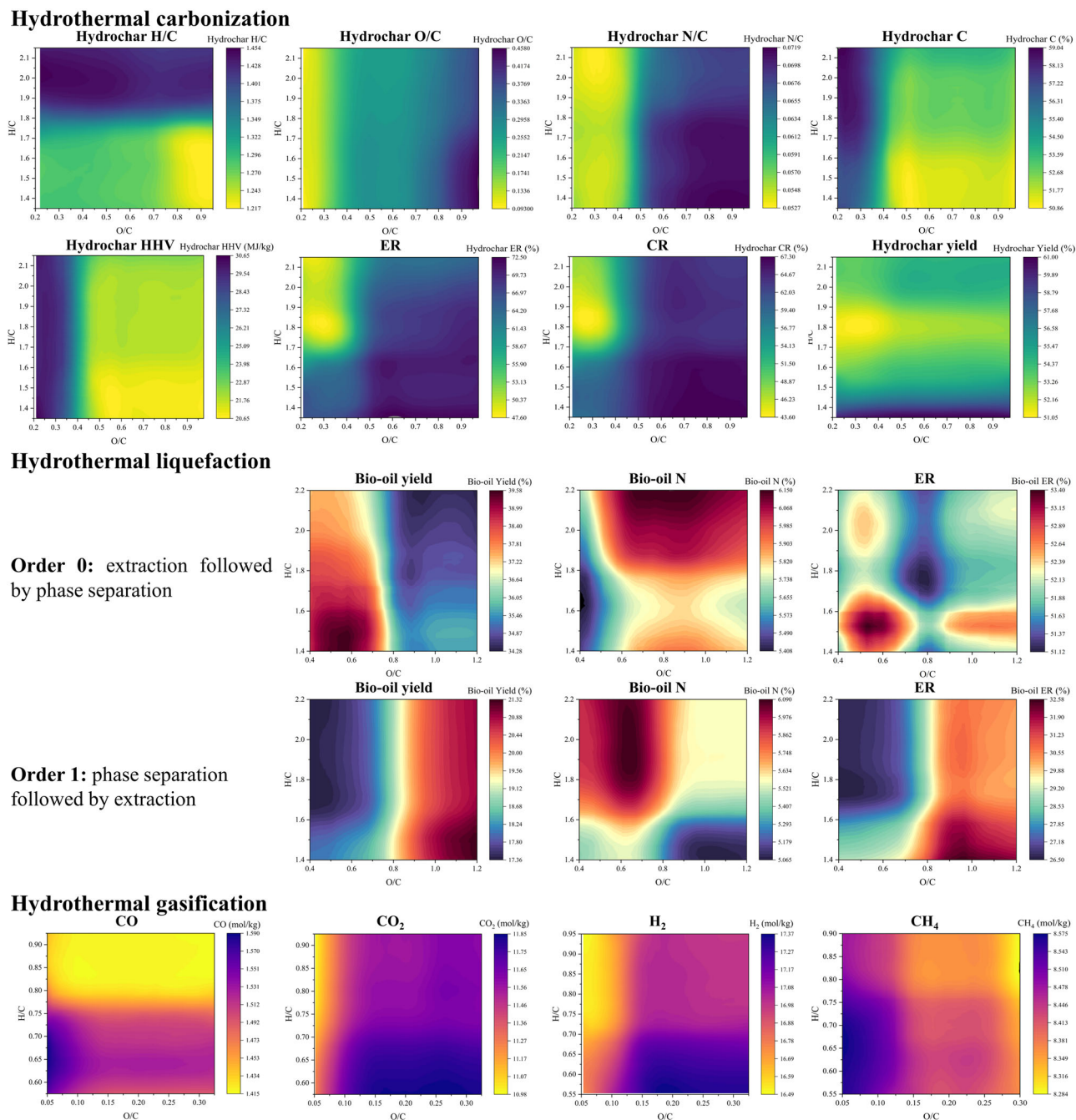


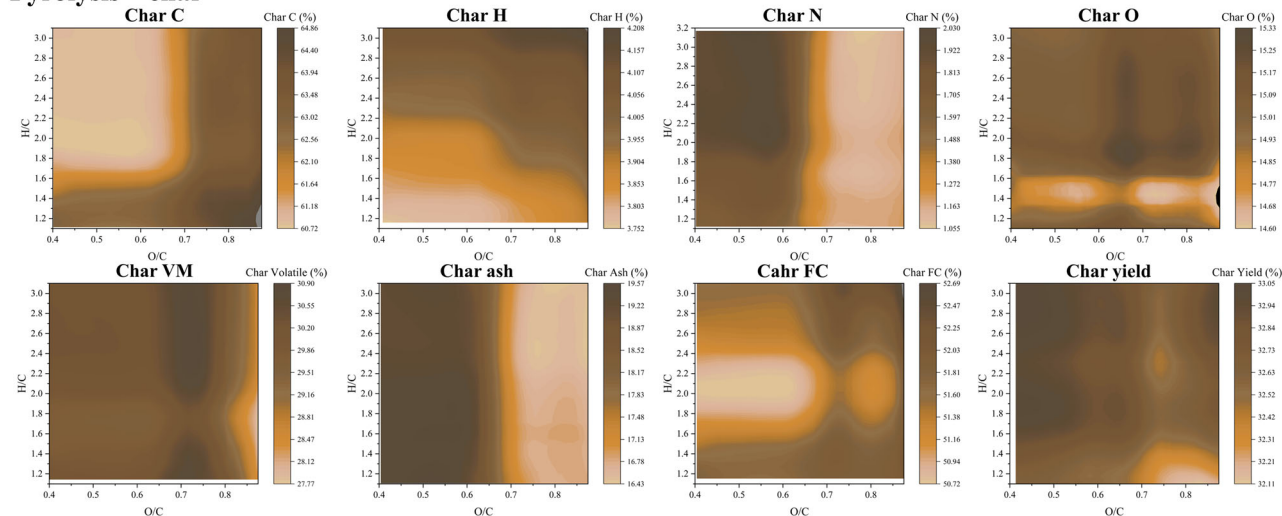
Fig. 3 Van Krevelen diagrams for hydrothermal carbonization (HTC), hydrothermal liquefaction (HTL), and hydrothermal gasification (HTG) processes. The HTC diagrams are established based on previous work by Li et al.⁷¹ using biodegradable waste such as sewage sludge, food waste, and manure as the investigated feedstock. The HTL diagrams are established based on previous work by Li et al.⁵⁵ using biomass and biodegradable waste, including algae, sludge, food waste, and manure as the investigated feedstock. The HTG diagrams are established based on previous work by Liu et al.⁷² using coal as the investigated feedstock. HHV higher heating value, ER energy recovery, CR carbon recovery.

The training data for HTC includes various types of biodegradable wastes. For food waste, different intermediates are produced during hydrolysis, with amino acids being the main intermediate after protein hydrolysis⁴⁴. These intermediates serve as substrates for producing heterocyclic compounds⁴⁵, particularly N-containing ring compounds⁴⁶, through Maillard reactions^{45,46}. This explains why using feedstocks located in regions with relatively high O/C ratios and relatively low H/C ratios results in the production of hydrochar with a higher N/C ratio. Additionally, sewage sludge typically contains significant

amounts of undigested proteins and extracellular polymeric substances from microbial aggregates^{47,48}.

In most empirical formulas, the HHV value is primarily determined by the C, H, and O contents. The C and H contents positively correlate with HHV value, while the O content has a negative correlation⁴⁹. The HTC HHV diagram aligns with these trends. The results in the HTC C diagram exhibit a similar trend to the results in the HTC HHV diagram, possibly due to the higher carbonization degree of hydrochar, which increases the influence of the C content on the HHV value. Consequently, the

Pyrolysis – char



Pyrolysis – bio-oil

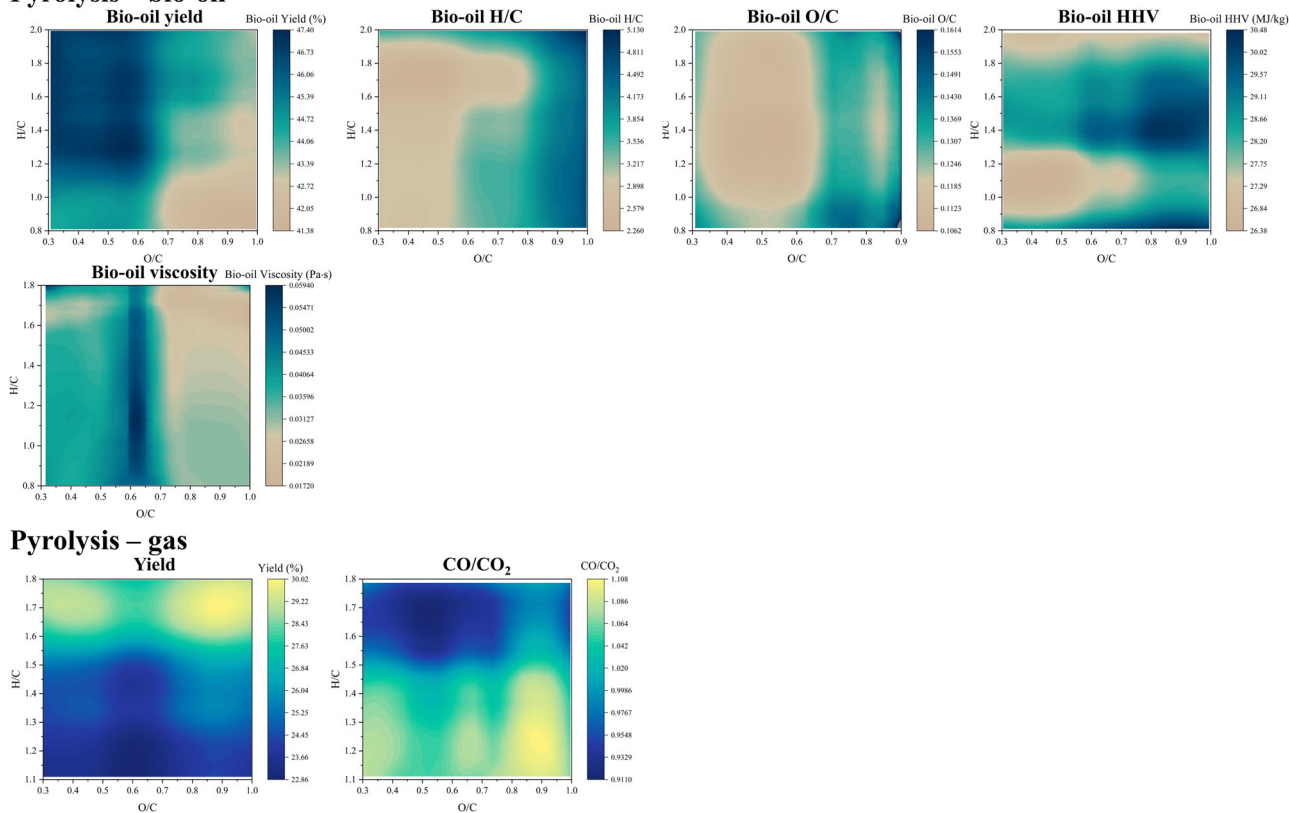


Fig. 4 Van Krevelen diagrams for the products of char, bio-oil, and gas yielded from pyrolysis. The char diagrams are established based on the previous work by Li et al.⁷³. The investigated feedstock is lignocellulosic biomass, including corncob, rice husk, sawdust, wood, etc. The bio-oil diagrams are established based on the previous work by Zhang et al.³⁶. The investigated feedstock is biomass, including seed, rice husk, algae, etc. The pyro-gas diagrams are established based on the previous work by Tang et al.⁷⁴. The investigated feedstock is biomass, including agriculture and forest waste, algae, etc. VM volatile matter, FC fix carbon.

HTC HHV diagram and the HTC C diagram share similarities. C content is important in predicting energy yields, as evidenced by the pattern observed in the HTC ER diagram, which mirrors the pattern in the HTC CR diagram. This similarity is not surprising, as the equations for calculating ER (Eq. 2) and CR (Eq. 3) depend linearly on the mass yield Eq. 1.

Lignin has a lower H/C ratio (1.14) compared to cellulose (1.67) and hemicellulose (1.60)⁵⁰. Therefore, a lower H/C ratio in lignocellulosic biodegradable waste indicates a relatively higher

lignin content. Lignin exhibits better thermal stability than cellulose and hemicellulose, which is reflected in the HTC Yield diagram: the lower the H/C ratio, the lower the yield. Similarly, the HTC C diagram illustrates that a lower H/C ratio results in lower C content in the hydrochar. The hydrochar produced from lignin has a relatively lower C content than that produced from cellulose and hemicellulose⁵¹. Hence, feedstock with a higher lignin content will have a lower H/C ratio and produce hydrochar with lower C content.

Hydrothermal liquefaction (HTL). The composition of the feedstock elements and compounds, as well as the order of product separation, play a crucial role in HTL⁵². Some small molecular compounds are considered as being light biocrude oil and can be extracted using organic solvents such as petroleum ether, dichloromethane, acetone, and ethyl acetate^{53,54}. In the original work⁵⁵, order 0 represents bio-oil extraction followed by phase separation, while order 1 represents the reverse process. Consequently, bio-oil obtained using order 1 mainly contains heavy organics, whereas bio-oil obtained using order 0 contains both light and heavy organics. As depicted in the HTL yield diagrams, the bio-oil yield and ER values of order 1 are relatively higher compared to those of order 0.

Both orders in HTL yield diagrams indicate that a low H/C in the feedstock favors bio-oil yield. However, the HTL yield diagram for order 0 shows that a low O/C contributes to a high bio-oil yield, while the opposite trend is observed in the HTL yield diagram for order 1. The main organics in biodegradable waste are carbohydrates, lipids, and proteins. Lipids have the relatively lowest O/C ratios⁵⁶ and the highest HTL bio-oil yield rates among these organics⁵⁷. Furthermore, the HTL of lipids produces more light organics than that of lignocelluloses and proteins^{58,59}. Consequently, a higher O/C ratio in the feedstock leads to a higher yield of heavy organics and a lower yield of light organics in the bio-oil.

Hydrothermal gasification (HTG). N₂, CO₂, H₂, CH₄, and CO are the main gases generated from HTG⁶⁰. HTG reactions are complex⁶¹, but the diagrams can be explained through the main reactions. The HTG diagrams for CO₂ and H₂ exhibit similar patterns because both gases are products of the reaction $C + 2H_2O \rightleftharpoons CO_2 + 2H_2$. Moreover, the H₂ and CH₄ diagrams exhibit a reverse pattern, which can be attributed to the reaction $C + 2H_2 \rightleftharpoons CH_4$.

A lower H/C ratio of a feedstock tends to result in a higher yield of CO, CO₂, and CH₄, as shown in the corresponding HTG diagrams. This can be explained by the requirement of C for the production of C-containing gases. Regarding the feedstock's O/C ratio, a lower O/C ratio increases the yields of CO and CH₄ while decreasing the yield of CO₂. A lower O/C ratio in the feedstock reduces the abundance of O and favors CH₄ production, while incomplete reactions produce CO instead of CO₂.

Pyrolysis

Pyrolysis-char. The pyrolysis-char H diagram demonstrates an apparent positive correlation between the H/C ratio of feedstock and the H content of char, as shown in Fig. 4. This can be attributed to feedstock's higher initial hydrogen content, resulting in more hydrogen residues in the solid products. However, the patterns observed in the other seven pyrolysis-char diagrams are challenging to explain. These results will be discussed in the section on "Reliability analysis" in Supplementary Note 6.

Pyrolysis-bio-oil. Pyrolysis-bio-oil Yield diagram shows that a higher H/C ratio and lower O/C ratio lead to increased bio-oil yields. Caprariis et al.⁶² observed that the use of oak wood with a high H/C ratio could generate a higher oil yield compared to the use of natural hay and walnut shell with low H/C ratios, which is in agreement with the result in the diagram.

The H/C and O/C diagrams for Pyrolysis-bio-oil highlight that the O/C ratio of the biomass predominantly influences the H/C and O/C ratios in the bio-oil. Generally, an elevation in the biomass's O/C ratio correspondingly increases the H/C and O/C ratios in the bio-oil. Cellulose and hemicellulose exhibit O/C ratios of 0.83 and 0.80, respectively. These values are noticeably

higher than lignin's O/C ratio, which stands at 0.35⁵⁰. Notably, bio-oil derived from the pyrolysis of cellulose and hemicellulose (xylan) demonstrated a superior H/C ratio compared to that from lignin pyrolysis⁶³. As a consequence, a higher O/C ratio in biomass, indicating a reduced lignin content, translates to a heightened H/C ratio in the resultant bio-oil.

The Pyrolysis-bio-oil HHV diagram shows that the bio-oil tends to have a relatively low HHV value when derived from biomass with low H/C (0.90–1.25) and O/C (0.30–0.75) ratios. However, the HHV of bio-oil reaches its maximum value for biomass with medium H/C (1.30–1.50) and high O/C (0.75–1.00) ratios. It should be noted that higher HHV values correspond to a higher economic value of bio-oil, as its combustion can generate more heat, providing meaningful guidance for the commercial applications of bio-oils derived from different types of biomasses.

The viscosity of bio-oils is more sensitive to the O/C ratio in the biomass, as is shown in the bio-oil Viscosity diagram. The bio-oil derived from biomass with O/C ratios ranging from 0.60 to 0.65 has a high viscosity, suggesting that the bio-oil has a high average molecular mass⁶⁴. Hence, biomass with an O/C ratio in this range is most recommended for producing bio-oil for lubricating oil applications. The pyrolysis of biomass with high H/C and O/C ratios can decrease the viscosity in the bio-oil, which agrees with the experimental observations by Fahmi et al.⁶⁴.

Pyrolysis-gas. Higher H/C and O/C values of feedstocks represent a higher potential for carbonization, resulting in a higher yield of pyro-gas, as shown by the Pyrolysis-gas Yield diagram. The main gases produced from biomass pyrolysis are CO₂, CO, H₂, and CH₄⁶⁵. Except for CO₂, the other three gases can be used as fuel. Therefore, it is desirable to minimize the yield of CO₂ when considering the pyro-gas. The production of CO₂ and CO is highly correlated. The CO/CO₂ ratio can be an important parameter for evaluating the fuel quality of a pyro-gas. The pyrolysis-gas CO/CO₂ diagram shows that the CO/CO₂ ratio is mainly determined by the feedstock's H/C ratio: the yield of CO can be higher than that of CO₂ when the feedstock's H/C is lower than approximately 1.5. The HTG CO diagram also shows a trend that a higher CO yield is correlated to a lower feedstock H/C, which can be explained by the high C content supplied from the feedstock.

Gasification. The Gasification Yield diagram suggests lower O/C and higher H/C values lead to higher syngas yields, as illustrated in Fig. 5. The diagram shows the highest syngas yield when O/C < 0.35 and H/C > 1.70, which typically represents the fuel compositions of plastic-rich waste materials⁶⁶. Similar findings have been reported in previous studies on biomass and waste gasification. For example, Arena et al.⁶⁷ studied the gasification of five different types of waste using a pilot-scale bubbling fluidized bed gasifier. They found that the waste fraction containing mostly plastics generated a higher syngas yield compared to the gasification of packaging waste, which had a lower plastic and higher lignocellulosic fraction.

The yield of CO in the syngas is directly proportional to the O/C content of the feedstock and does not vary significantly with different H/C values, as is shown in the Gasification CO diagram. Gasification of feedstock containing oxygenated compounds (with higher O/C ratios) produces more CO⁶⁸. On the other hand, the relationship between the CO₂ yield and the H/C and O/C ratios of the feedstock is more complex, as depicted in the Gasification CO₂ diagram. To minimize the generation of CO₂ in the syngas, feedstock with O/C ratios between approximately 0.35 and 0.45 should be used, while the production of CO₂ is likely to increase when the O/C value is outside that range.

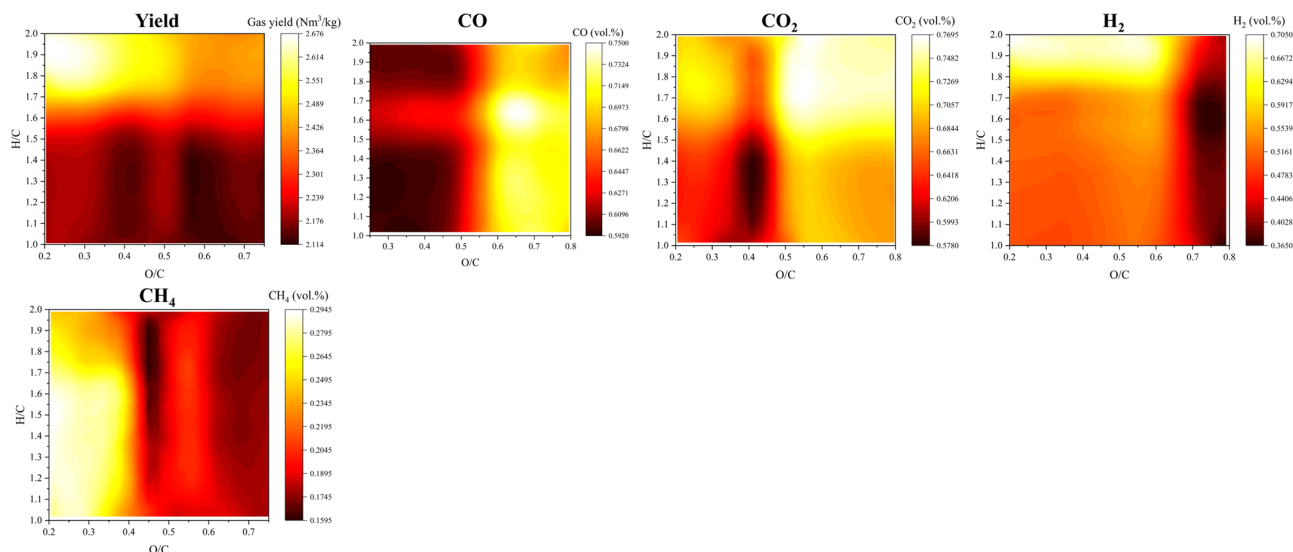


Fig. 5 Van Krevelen diagrams for the gas products of gasification. The gasification diagrams are established based on the previous work by Serrano et al.⁷⁵. The investigated feedstock is lignocellulosic biomass and plastics.

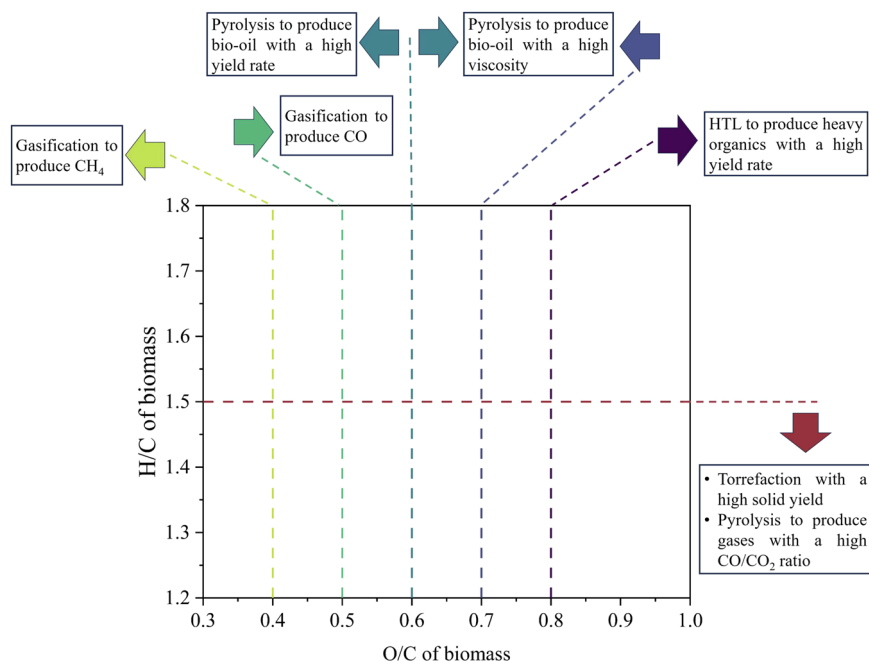


Fig. 6 Summary of recommendations for the thermal conversion of biomass to achieve different targets, illustrated using a Van Krevelen diagram. Only models created from datasets containing biomass feedstock are included.

In the Gasification H_2 diagram, at $O/C < 0.6$, higher H/C values in biomass result in higher H_2 yields. However, at $O/C > 0.6$, higher H/C values do not always correspond to higher H_2 yield. Instead, the value decreases significantly and remains relatively constant at different H/C values. This observation aligns with previous studies on fluidized bed gasification of biomass and plastic waste, which have shown that increasing the H/C ratio by increasing the plastic fraction in biomass-plastic fuel mixtures generally leads to a higher H_2 generation⁶⁸.

The Gasification CH_4 diagram follows a similar trend to the gasification diagram of H_2 , reaching its higher level when the feedstock has lower O/C values. The production of CH_4 during waste gasification is linked to the fundamental components of the waste materials. Long-chain hydrocarbon compounds in plastics

undergo cracking and reforming reactions during gasification, resulting in the formation of lighter hydrocarbon gases such as CH_4 and C_2H_4 ⁶⁹. This process explains why the yield of CH_4 is higher during the gasification of high H/C feedstock, such as plastics.

Summary of biomass thermal conversions. A brief summary is provided in this section, outlining recommendations for the thermal conversion of biomass with varying H/C and O/C ratios to achieve different target products. Notably, ML models for torrefaction, HTL, pyrolysis-bio-oil, pyrolysis-gas, and gasification were built using datasets from biomass feedstock. The insights from these models can be succinctly represented on a van Krevelen diagram, as depicted in Fig. 6.

- When aiming for a high solid yield, lignocellulosic biomass with an H/C ratio greater than 1.5 and biodegradable waste with an H/C ratio greater than 1.4 are not recommended for conversion via torrefaction and hydrothermal carbonization, respectively. Additionally, biodegradable waste with an O/C ratio lower than 0.4 is ideally treated using HTC to yield hydrochar with a high HHV.
- Biodegradable waste and biomass possessing an O/C ratio above 0.8 could be converted using HTL to achieve a substantial yield of heavy organics.
- HTG processing of coal with an O/C ratio below approximately 0.10 tends to favor the production of CO and CH₄. However, when the O/C ratio exceeds 0.1, the production of H₂ and CO₂ is more prevalent.
- For biomass with an O/C ratio less than approximately 0.6, pyrolysis is the recommended treatment to yield a high quantity of bio-oil. Conversely, biomass with an O/C ratio ranging from about 0.6 to 0.7 has the potential to produce bio-oil with increased viscosity.
- Biomass exhibiting a H/C ratio of less than approximately 1.5 can undergo pyrolysis to produce superior-quality pyro-gas, characterized by a high CO/CO₂ ratio.
- The CH₄ content in gases stemming from biomass gasification can be augmented when the biomass's O/C is less than 0.4. Conversely, a higher CO content is achieved when the biomass's O/C exceeds 0.5.

Conclusions

We have constructed a series of van Krevelen diagrams to visually illustrate the relationships between feedstocks and products in thermal conversion techniques including torrefaction, hydrothermal carbonization, hydrothermal liquefaction, hydrothermal gasification, pyrolysis, and gasification. The reliability of these diagrams is evaluated based on the model's accuracy and the significance of the H/C and O/C parameters. Interestingly, the diagrams exhibit a peculiar pattern associated with low-reliability performance, particularly in the case of pyrolysis-char diagrams.

These diagrams contribute to a better understanding of the respective thermal processes and provide valuable insights for decision-making in practical scenarios. Specifically, they assist in the selection of an appropriate thermal treatment method for a specific feedstock, thereby optimizing the overall performance of the thermal process by considering the blending of different feedstocks to achieve optimal H/C and O/C ratios. By utilizing these diagrams, stakeholders can make informed choices and maximize the efficiency of thermal conversion processes.

In addition to the feedstock-product relationship, the feedstock-reaction connection is also of great importance. The same methodology can be applied to create diagrams that illustrate the relationship between the feedstock and pyrolytic activation energy (Supplementary Note 5). Therefore, further investigation to establish a series of diagrams expressing the feedstock-reaction relationship is of significant interest.

Methods

The present study builds upon the databases, methods, and findings of eight previous works that specifically investigated ML in the context of torrefaction⁷⁰, hydrothermal carbonization (HTC)⁷¹, hydrothermal liquefaction (HTL)⁵⁵, hydrothermal gasification (HTG)⁷², pyrolysis^{36,73,74}, and gasification⁷⁵. The referred works and their input and output parameters are given in Table 1.

Table 1 Summary of referred previous works.

Process	Feedstock	Product	Input parameter	Output parameter
Torrefaction	Lignocellulosic biomass	Torrefied biomass ⁷⁰ Hydrochar ⁷¹	C, H, N, ash, VM, size, time, T, CO ₂ , O ₂	Yield Yield, C, H/C, O/C, N/C, CR, ER, HHV Yield, N, ER
Hydrothermal carbonization	Biodegradable waste	Bio-oil ⁵⁵	C, H, N, O, FC, ash, VM, time, T, WC	H ₂ , CO, CH ₄ , CO ₂
Hydrothermal liquefaction	Biodegradable waste & biomass	Gas ⁷²	C, H, N, O, S, ash, protein, lipid, carbohydrate, time, T, extraction order	Yield, C, H, N, O, FC, ash, VM
Hydrothermal gasification	Coal	Char ⁷³	C, H, N, O, S, FC, ash, VM, moisture, time, T, ER, CON	Yield, C, H, N, O, FC, ash, VM
Pyrolysis	Lignocellulosic Biomass	Bio-oil ³⁶	C, H, N, O, FC, ash, VM, time, T, HR	Yield, H/C, O/C, HHV, viscosity
Pyrolysis	Biomass	Gas ⁷⁴ Gas ⁷⁵	C, H, N, O, FC, ash, VM, size, T, HR, room temperature C, H, N, O, FC, ash, VM, size, T, HR, FR C, H, O, ash, moisture, ER, T, steam/biomass ratio, bed material	Yield, CO, CO ₂ , H ₂ , CH ₄ Yield, H ₂ , CH ₄ , CO, CO ₂

VM volatile matter, T temperature, FC fix carbon, WC water content of HTC process, CR carbon recovery, HHV higher heating value, ER energy recovery, HTL hydrothermal liquefaction, HTC hydrothermal carbonization, HTG hydrothermal gasification, HTL hydrothermal liquefaction, ER energy recovery, FR flow rate.

Mass yield (Yield) is typically determined directly using a well-established equation:

$$\text{Yield} = \frac{m_{\text{dry product}}}{m_{\text{dry feedstock}}} \quad (1)$$

The energy recovery (ER) is defined as follows⁴⁴:

$$\text{ER} = \text{Yield} \cdot \frac{\text{HHV}_{\text{product}}}{\text{HHV}_{\text{feedstock}}} \quad (2)$$

The carbon recovery (CR) has been determined using the following equation⁷¹:

$$\text{CR} = Y_m \cdot \frac{\text{Carbon content}_{\text{product}}}{\text{Carbon content}_{\text{feedstock}}} \quad (3)$$

These previous works have demonstrated the feasibility and reliability of utilizing the datasets they employed to develop robust ML models for the respective thermal conversion processes. By leveraging the insights and findings from these prior studies, we have been able to enhance our understanding and analysis of thermal conversion processes through the application of ML techniques. Specifically in this study, we have engineered some features and targets for a better conclusion. These changes include:

1. Converting the contents of H and O to the atomic ratios of H/C and O/C, respectively.
2. Some minor revisions of the datasets where the former researchers made some mistakes.
3. For the pyrolysis-gas models, we investigate the outputs of yield and the atomic ratio of CO/CO₂.

The original datasets and their preliminary analysis can be obtained from the sources cited in the respective papers or can be requested from the authors directly. These datasets serve as a foundation for our work and have been modified to improve the consistency and accuracy of our analyses.

Among the eight referenced studies, the random forest method has been implemented most frequently, with a testing R² value greater than 0.75 (as shown in Fig. 1). To establish a set of general diagrams for different thermal conversion processes, we consistently employ the random forest regressor for generation of the 3D van Krevelen diagrams.

To generate the van Krevelen diagram, a two-way partial dependence analysis is performed based on the constructed model, focusing on the H/C and O/C ratios. The reliability of the produced diagram is highest within the ranges where the training data is most abundant. Therefore, appropriate ranges for H/C and O/C are determined by evaluating the kernel density of the training data distribution (Supplementary Note 7).

During the analysis, all other input parameters are set to their mean values from the training dataset. The resulting two-way partial dependence plots represent the predicted outcomes under specific input conditions. To obtain a van Krevelen diagram that can represent the relationship between feedstock and product more generally, smoothing is applied to the original two-way partial dependence plots (Supplementary Fig. 5).

Data availability

The data that support the findings of this study are available from the corresponding author upon reasonable request. The information on the dataset used for training biomass torrefaction machine learning model is given in Supplementary Data 1.

Code availability

In the conduct of this study, we utilized the Random Forest algorithm as implemented in the Scikit-Learn Python library, version 0.23.1. We would like to acknowledge the

developers of Scikit-Learn for providing this valuable resource openly. The algorithm was used in its original form without any modifications, ensuring the reproducibility and integrity of our research. For further reference, the library can be accessed at <https://scikit-learn.org/0.23/>.

Received: 16 June 2023; Accepted: 27 November 2023;

Published online: 13 December 2023

References

1. Akhtar, A., Krepl, V. & Ivanova, T. A combined overview of combustion, pyrolysis, and gasification of biomass. *Energy Fuels* **32**, 7294–7318 (2018).
2. Gao, N., Kamran, K., Quan, C. & Williams, P. T. Thermochemical conversion of sewage sludge: a critical review. *Prog. Energy Combust. Sci.* **79**, 100843 (2020).
3. Lee, J., Kim, S., You, S. & Park, Y.-K. Bioenergy generation from thermochemical conversion of lignocellulosic biomass-based integrated renewable energy systems. *Renew. Sustain. Energy Rev.* **178**, 113240 (2023).
4. Asghar, U. et al. Review on the progress in emission control technologies for the abatement of CO₂, SO_x and NO_x from fuel combustion. *J. Environ. Chem. Eng.* **9**, 106064 (2021).
5. Goyal, H., Seal, D. & Saxena, R. Bio-fuels from thermochemical conversion of renewable resources: a review. *Renew. Sustain. Energy Rev.* **12**, 504–517 (2008).
6. Kumar, G. et al. A review of thermochemical conversion of microalgal biomass for biofuels: chemistry and processes. *Green Chem.* **19**, 44–67 (2017).
7. Siwal, S. S. et al. Advanced thermochemical conversion technologies used for energy generation: advancement and prospects. *Fuel* **321**, 124107 (2022).
8. Van Krevelen, D. Graphical-statistical method for the study of structure and reaction processes of coal. *Fuel* **29**, 269–284 (1950).
9. Laszakovits, J. R. & MacKay, A. A. Data-based chemical class regions for Van Krevelen diagrams. *J. Am. Soc. Mass Spectrom.* **33**, 198–202 (2021).
10. Prins, M. J., Ptasiński, K. J. & Janssen, F. J. From coal to biomass gasification: comparison of thermodynamic efficiency. *Energy* **32**, 1248–1259 (2007).
11. Rivas-Ubach, A. et al. Moving beyond the van Krevelen diagram: a new stoichiometric approach for compound classification in organisms. *Anal. Chem.* **90**, 6152–6160 (2018).
12. Danger, G. et al. Exploring the link between molecular cloud ices and chondritic organic matter in laboratory. *Nat. Commun.* **12**, 3538 (2021).
13. McDonough, L. K. et al. A new conceptual framework for the transformation of groundwater dissolved organic matter. *Nat. Commun.* **13**, 2153 (2022).
14. Yu, S. et al. Decoupled temperature and pressure hydrothermal synthesis of carbon sub-micron spheres from cellulose. *Nat. Commun.* **13**, 3616 (2022).
15. Chen, H. et al. Mesophilic and thermophilic anaerobic digestion of aqueous phase generated from hydrothermal liquefaction of cornstalk: molecular and metabolic insights. *Water Res.* **168**, 115199 (2020).
16. Qamrani, N. A., Rahman, M. M., Won, S., Shim, S. & Ra, C. Biochar properties and eco-friendly applications for climate change mitigation, waste management, and wastewater treatment: a review. *Renew. Sustain. Energy Rev.* **79**, 255–273 (2017).
17. Herzsprung, P. et al. Improved understanding of dissolved organic matter processing in freshwater using complementary experimental and machine learning approaches. *Environ. Sci. Technol.* **54**, 13556–13565 (2020).
18. Martins, N. et al. Revisiting 3D van Krevelen diagrams as a tool for the visualization of volatile profile of varietal olive oils from Alentejo region, Portugal. *Talanta* **207**, 120276 (2021).
19. Ollivier, S. et al. New insights into the Van Krevelen diagram: automated molecular formula determination from HRMS for a large chemical profiling of lichen extracts. *Phytochem. Anal.* **33**, 1111–1120 (2022).
20. Chew, J. J. & Doshi, V. Recent advances in biomass pretreatment—torrefaction fundamentals and technology. *Renew. Sustain. Energy Rev.* **15**, 4212–4222 (2011).
21. Weiner, B., Poerschmann, J., Wedwitschka, H., Koehler, R. & Kopinke, F.-D. Influence of process water reuse on the hydrothermal carbonization of paper. *ACS Sustain. Chem. Eng.* **2**, 2165–2171 (2014).
22. Abomohra, A. E.-F., Sheikh, H. M., El-Naggar, A. H. & Wang, Q. Microwave vacuum co-pyrolysis of waste plastic and seaweeds for enhanced crude bio-oil recovery: experimental and feasibility study towards industrialization. *Renew. Sustain. Energy Rev.* **149**, 111335 (2021).
23. Hungsberg, M. et al. Thermodynamic equilibrium investigation to operational capabilities and process tolerance of plasma gasification for various feedstock. *Chem. Eng. Sci.* **250**, 117401 (2022).
24. Kim, S., Kramer, R. W. & Hatcher, P. G. Graphical method for analysis of ultrahigh-resolution broadband mass spectra of natural organic matter, the van Krevelen diagram. *Anal. Chem.* **75**, 5336–5344 (2003).

25. Wu, Z., Rodgers, R. P. & Marshall, A. G. Two-and three-dimensional van Krevelen diagrams: a graphical analysis complementary to the Kendrick mass plot for sorting elemental compositions of complex organic mixtures based on ultrahigh-resolution broadband Fourier transform ion cyclotron resonance mass measurements. *Anal. Chem.* **76**, 2511–2516 (2004).
26. Lozano, D. C. P., Jones, H. E., Reina, T. R., Volpe, R. & Barrow, M. P. Unlocking the potential of biofuels via reaction pathways in van Krevelen diagrams. *Green Chem.* **23**, 8949–8963 (2021).
27. Herzsprung, P. et al. Variations of DOM quality in inflows of a drinking water reservoir: linking of van Krevelen diagrams with EEMF spectra by rank correlation. *Environ. Sci. Technol.* **46**, 5511–5518 (2012).
28. Qiu, Y. et al. Effects of cellulose-lignin interaction on the evolution of biomass pyrolysis bio-oil heavy components. *Fuel* **323**, 124413 (2022).
29. Akhtar, A., Jiříček, I., Ivanova, T., Mehraabadi, A. & Krepl, V. Carbon conversion and stabilisation of date palm and high rate algal pond (microalgae) biomass through slow pyrolysis. *Int. J. Energy Res.* **43**, 4403–4416 (2019).
30. Yang, K. et al. Secondary reactions of primary tar from biomass pyrolysis: characterization of heavy products by FT-ICR MS. *Energy Fuels* **35**, 13191–13199 (2021).
31. Wang, S. et al. Effect of hydrothermal carbonization pretreatment on the pyrolysis behavior of the digestate of agricultural waste: a view on kinetics and thermodynamics. *Chem. Eng. J.* **431**, 133881 (2022).
32. Jordan, M. I. & Mitchell, T. M. Machine learning: trends, perspectives, and prospects. *Science* **349**, 255–260 (2015).
33. Naqvi, S. R. et al. Applications of machine learning in thermochemical conversion of biomass—a review. *Fuel* **332**, 126055 (2023).
34. Seo, M. W. et al. Recent advances of thermochemical conversion processes for biorefinery. *Bioresour. Technol.* **343**, 126109 (2022).
35. Greenwell, B. M. pdr: an R Package for constructing partial dependence plots. *R. J.* **9**, 421 (2017).
36. Zhang, T. et al. Machine learning prediction of bio-oil characteristics quantitatively relating to biomass compositions and pyrolysis conditions. *Fuel* **312**, 122812 (2022).
37. Chen, W.-H. et al. Progress in biomass torrefaction: principles, applications and challenges. *Prog. Energy Combust. Sci.* **82**, 100887 (2021).
38. Du, S.-W., Chen, W.-H. & Lucas, J. A. Pretreatment of biomass by torrefaction and carbonization for coal blend used in pulverized coal injection. *Bioresour. Technol.* **161**, 333–339 (2014).
39. Thengane, S. K., Kung, K. S., Gomez-Barea, A. & Ghoniem, A. F. Advances in biomass torrefaction: parameters, models, reactors, applications, deployment, and market. *Prog. Energy Combust. Sci.* **93**, 101040 (2022).
40. Martínez, M. G. et al. Torrefaction of cellulose, hemicelluloses and lignin extracted from woody and agricultural biomass in TGA-GC/MS: linking production profiles of volatile species to biomass type and macromolecular composition. *Ind. Crops Prod.* **176**, 114350 (2022).
41. Zheng, A. et al. Impact of torrefaction on the chemical structure and catalytic fast pyrolysis behavior of hemicellulose, lignin, and cellulose. *Energy Fuels* **29**, 8027–8034 (2015).
42. Chen, D. et al. Investigation of biomass torrefaction based on three major components: hemicellulose, cellulose, and lignin. *Energy Convers. Manag.* **169**, 228–237 (2018).
43. Kruse, A., Funke, A. & Titirici, M.-M. Hydrothermal conversion of biomass to fuels and energetic materials. *Curr. Opin. Chem. Biol.* **17**, 515–521 (2013).
44. Sharma, H. B., Panigrahi, S. & Dubey, B. K. Food waste hydrothermal carbonization: study on the effects of reaction severities, pelletization and framework development using approaches of the circular economy. *Bioresour. Technol.* **333**, 125187 (2021).
45. Wang, L. et al. Hydrothermal treatment of food waste for bio-fertilizer production: formation and regulation of humus substances in hydrochar. *Sci. Total Environ.* **838**, 155900 (2022).
46. Djandja, O. S., Yin, L.-X., Wang, Z.-C. & Duan, P.-G. From wastewater treatment to resources recovery through hydrothermal treatments of municipal sewage sludge: a critical review. *Process Saf. Environ. Prot.* **151**, 101–127 (2021).
47. Inoue, S., Sawayama, S., Ogi, T. & Yokoyama, S.-Y. Organic composition of liquidized sewage sludge. *Biomass Bioenergy* **10**, 37–40 (1996).
48. Sheng, G.-P., Yu, H.-Q. & Li, X.-Y. Extracellular polymeric substances (EPS) of microbial aggregates in biological wastewater treatment systems: a review. *Biotechnol. Adv.* **28**, 882–894 (2010).
49. Channiwal, S. & Parikh, P. A unified correlation for estimating HHV of solid, liquid and gaseous fuels. *Fuel* **81**, 1051–1063 (2002).
50. Wang, S. et al. A machine learning model to predict the pyrolytic kinetics of different types of feedstocks. *Energy Convers. Manag.* **260**, 115613 (2022).
51. Kang, S., Li, X., Fan, J. & Chang, J. Characterization of hydrochars produced by hydrothermal carbonization of lignin, cellulose, D-xylose, and wood meal. *Ind. Eng. Chem. Res.* **51**, 9023–9031 (2012).
52. Xu, Y. et al. Understand the antibacterial behavior and mechanism of hydrothermal wastewater. *Water Res.* **226**, 119318 (2022).
53. Chen, H. et al. Biogas production from hydrothermal liquefaction wastewater (HTLWW): focusing on the microbial communities as revealed by high-throughput sequencing of full-length 16S rRNA genes. *Water Res.* **106**, 98–107 (2016).
54. Fernandez, S., Srinivas, K., Schmidt, A. J., Swita, M. S. & Ahring, B. K. Anaerobic digestion of organic fraction from hydrothermal liquefied algae wastewater byproduct. *Bioresour. Technol.* **247**, 250–258 (2018).
55. Li, J. et al. Machine learning aided bio-oil production with high energy recovery and low nitrogen content from hydrothermal liquefaction of biomass with experiment verification. *Chem. Eng. J.* **425**, 130649 (2021).
56. Lu, J., Watson, J., Liu, Z. & Wu, Y. Elemental migration and transformation during hydrothermal liquefaction of biomass. *J. Hazard. Mater.* **423**, 126961 (2022).
57. Lu, J., Liu, Z., Zhang, Y. & Savage, P. E. Synergistic and antagonistic interactions during hydrothermal liquefaction of soybean oil, soy protein, cellulose, xylose, and lignin. *ACS Sustain. Chem. Eng.* **6**, 14501–14509 (2018).
58. Xu, Y., Lu, J., Wang, Y., Yuan, C. & Liu, Z. Construct a novel anti-bacteria pool from hydrothermal liquefaction aqueous family. *J. Hazard. Mater.* **423**, 127162 (2022).
59. Chen, W.-T. et al. Co-liquefaction of swine manure and mixed-culture algal biomass from a wastewater treatment system to produce bio-crude oil. *Appl. Energy* **128**, 209–216 (2014).
60. Hao, W. Q. & Liu, X. J. Molecular dynamics investigation on the co-gasification of various components of sewage sludge in supercritical water. *Fuel* **334**, 126729 (2023).
61. Okolie, J. A. et al. Modeling and process optimization of hydrothermal gasification for hydrogen production: a comprehensive review. *J. Supercrit. Fluids* **173**, 105199 (2021).
62. De Caprariis, B., De Filippis, P., Petrullo, A. & Scarsella, M. Hydrothermal liquefaction of biomass: influence of temperature and biomass composition on the bio-oil production. *Fuel* **208**, 618–625 (2017).
63. Rutkowski, P. Pyrolysis of cellulose, xylan and lignin with the K₂CO₃ and ZnCl₂ addition for bio-oil production. *Fuel Process. Technol.* **92**, 517–522 (2011).
64. Fahmi, R., Bridgwater, A. V., Donnison, I., Yates, N. & Jones, J. The effect of lignin and inorganic species in biomass on pyrolysis oil yields, quality and stability. *Fuel* **87**, 1230–1240 (2008).
65. Kan, T., Strezov, V. & Evans, T. J. Lignocellulosic biomass pyrolysis: a review of product properties and effects of pyrolysis parameters. *Renew. Sustain. Energy Rev.* **57**, 1126–1140 (2016).
66. Yu, D., Hui, H., Ding, G., Dong, N. & Li, S. Enhancement of aromatics production from catalytic co-pyrolysis of walnut shell and LDPE via a two-step approach. *J. Anal. Appl. Pyrolysis* **157**, 105216 (2021).
67. Arena, U., Zaccariello, L. & Mastellone, M. L. Fluidized bed gasification of waste-derived fuels. *Waste Manag.* **30**, 1212–1219 (2010).
68. Wilk, V. & Hofbauer, H. Co-gasification of plastics and biomass in a dual fluidized-bed steam gasifier: possible interactions of fuels. *Energy Fuels* **27**, 3261–3273 (2013).
69. Zaini, I. N. et al. Production of H₂-rich syngas from excavated landfill waste through steam co-gasification with biochar. *Energy* **207**, 118208 (2020).
70. Onsee, T. & Tippayawong, N. Machine learning application to predict yields of solid products from biomass torrefaction. *Renew. Energy* **167**, 425–432 (2021).
71. Li, J. et al. Multi-task prediction and optimization of hydrochar properties from high-moisture municipal solid waste: application of machine learning on waste-to-resource. *J. Clean. Prod.* **278**, 123928 (2021).
72. Liu, S. et al. Predicting gas production by supercritical water gasification of coal using machine learning. *Fuel* **329**, 125478 (2022).
73. Li, Y., Gupta, R. & You, S. Machine learning assisted prediction of biochar yield and composition via pyrolysis of biomass. *Bioresour. Technol.* **359**, 127511 (2022).
74. Tang, Q. et al. Machine learning prediction of pyrolytic gas yield and compositions with feature reduction methods: effects of pyrolysis conditions and biomass characteristics. *Bioresour. Technol.* **339**, 125581 (2021).
75. Serrano, D., Golpour, I. & Sánchez-Delgado, S. Predicting the effect of bed materials in bubbling fluidized bed gasification using artificial neural networks (ANNs) modeling approach. *Fuel* **266**, 117021 (2020).

Acknowledgements

The financial support of the foundation of Jiangsu Key Lab of Biomass Energy and Material (JSBEM-S-202101) is appreciated. S.W. would like to thank the support of the Research Fund for High-level Talents Introduction of Nanjing Forestry University. Y.W. would like to thank the financial support from (1) the European Commission and the Swedish Research Council Formas for funding in the frame of the collaborative international consortium (RECOWATDIG) financed under the 2018 Joint call of the

WaterWorks2017 ERA-NET Cofund and (2) the National Research Foundation, Singapore, and A*STAR under its Low-Carbon Energy Research (LCER) Funding Initiative (FI) Project (U2102d2011, WBS: A-8000278-00-00).

Author contributions

Conceptualization: Y.Wen. Methodology: S.W., Z.S., Y.Wen. Software: S.W., Z.S., Y.Wen. Formal analysis: Y.Wang, Y.Wen. Investigation: S.W., Z.S., Y.Wen. Resources: T.O., N.T. Writing—original draft: S.W. (pyro-gas), Z.S. (pyro-char), Y.Wen (overall), L.N. (HTC and torrefaction), R.P. (pyro-bio-oil), Y.X. (HTL & HTG), I.N.Z. (gasification), K.J. (torrefaction), C.A.-B. (HTC). Writing—review & editing: S.W., Y.Wen, L.N., I.N.Z., K.J., C.A.-B., T.O., P.G.J., W.Y. Visualization: Y.Wang, Y.Wen, C.T. Supervision: H.P.-K., P.G.J., W.Y., K.S., J.J., S.K., C.-H.W. Project administration: Y.Wen. Funding acquisition: H.P.-K., P.G.J., W.Y., K.S., J.J., S.K., C.-H.W.

Competing interests

The authors declare no competing interests.

Additional information

Supplementary information The online version contains supplementary material available at <https://doi.org/10.1038/s42004-023-01077-z>.

Correspondence and requests for materials should be addressed to Yuming Wen, Jianchun Jiang, Sibudjing Kawi or Chi-Hwa Wang.

Peer review information *Communications Chemistry* thanks Mark Mba-Wright, Mojtaba Hedayati Marzbali and the other anonymous reviewers for their contribution to the peer review of this work. A peer review file is available.

Reprints and permission information is available at <http://www.nature.com/reprints>

Publisher's note Springer Nature remains neutral with regard to jurisdictional claims in published maps and institutional affiliations.



Open Access This article is licensed under a Creative Commons Attribution 4.0 International License, which permits use, sharing, adaptation, distribution and reproduction in any medium or format, as long as you give appropriate credit to the original author(s) and the source, provide a link to the Creative Commons licence, and indicate if changes were made. The images or other third party material in this article are included in the article's Creative Commons licence, unless indicated otherwise in a credit line to the material. If material is not included in the article's Creative Commons licence and your intended use is not permitted by statutory regulation or exceeds the permitted use, you will need to obtain permission directly from the copyright holder. To view a copy of this licence, visit <http://creativecommons.org/licenses/by/4.0/>.

© The Author(s) 2023